

Growth of ZnSe nano and microstructures at high vacuum by thermal evaporation

D. Yuvaraj · R. Rakesh Kumar · V. Tamil Selvan ·
M. Sathyanarayanan · K. Narasimha Rao

Received: 16 February 2013 / Accepted: 1 April 2013 / Published online: 17 April 2013
© The Author(s) 2013. This article is published with open access at Springerlink.com

Abstract ZnSe nano and microstructures were grown on Si substrates in high vacuum by thermal evaporation at different source temperatures ranging from 850 to 950 °C. Morphology, chemical composition and structural properties of these grown ZnSe nano and microstructures were studied using scanning electron microscope (SEM) and transmission electron microscope (TEM). SEM studies revealed that the morphology of grown structures contains nanowires, nanobelts and microcrystals. TEM studies showed that the grown nanowires and nanobelts are single crystalline in nature with growth direction along [110] of zinc blende structure. The room temperature photoluminescence (PL) spectra of these nanostructures grown at different temperatures exhibited a strong broad defect level (DL) emission peak and a weak narrow near band edge (NBE) emission peak. Further, the intensity of DL emission peak was found to increase with increase in source temperature.

Keywords Thermal evaporation · ZnSe · Nanobelt · Nanowire · Vapor–Solid growth mechanism · Photoluminescence

Introduction

In recent years, the research interest on growth of semiconductor nanostructures has largely increased, due to their interesting physical and chemical properties (Pal 1999). ZnSe, a direct band gap (2.8 eV) II–VI semiconductor with large exciton binding energy (21 meV), has been investigated for potential applications in optoelectronic devices such as light emitting diodes and laser diodes (Katayama et al. 1998). ZnSe nanostructures with different morphologies such as wires, belts, rods and tetrapods have been synthesized by different techniques such as vapor transport, metal–organic chemical vapor deposition (MOCVD), molecular beam epitaxy (MBE) and solution growth (Ye et al. 2004; Leung et al. 2006; Shan et al. 2006; Cai et al. 2006; Mazher et al. 2004). Among these techniques, vapor transport technique is more popular due to its simplicity in growing single crystalline nanostructures with different morphologies (Ye et al. 2004; Leung et al. 2006). In the conventional vapor transport process, nanostructures were grown in a horizontally aligned tubular furnace at relatively low vacuum ($\sim 10^{-2}$ mbar to atmosphere) and in the presence of carrier gas and catalyst (Ye et al. 2004; Leung et al. 2006). Inclusion of carrier gas and catalytic particles into the grown nanostructures is the main drawback of this technique. These added impurities significantly affect the optical and electronic properties of the grown nanostructures. Xiang et al. (2003) reported that the inclusion of Au catalyst into ZnSe nanowire results in strong green emission from the nanowire. Philipose et al. (2008) reported that the ZnSe nanostructures grown in low vacuum condition exhibits stronger DL emissions than the much needed NBE emission for optoelectronic applications. Further, ZnSe nanowires grown by CVD under low vacuum conditions have unusual PL emission due to the

D. Yuvaraj · R. Rakesh Kumar · V. Tamil Selvan ·
K. Narasimha Rao
Department of Instrumentation and Applied Physics,
Indian Institute of Science, Bangalore 560012, India

M. Sathyanarayanan
Department of Physics, Anna University, Chennai 600025, India

D. Yuvaraj (✉)
Department of Electrical Engineering, London Centre for
Nanotechnology, University College London, London, UK
e-mail: yuvaraj@gmail.com

formation of oxide layer on its surface (Shen et al. 2006). Therefore, in order to grow ZnSe nanostructures with good optoelectronic properties, a technique involving high vacuum and metal-catalyst-free growth is required.

In this work, ZnSe nano and microstructures were grown on Si substrates by thermal evaporation in high vacuum (10^{-3} Pa) without employing metal catalyst. ZnSe evaporated from the tantalum boat condenses on the Si substrate placed above the boat, and grows into different nano and microstructures. The morphology, microstructure, composition and optical properties of the grown nanostructures were studied by SEM, TEM, XRD and PL. The possible mechanism behind the growth of the ZnSe nano and microstructures has been discussed in detail in this report.

Experimental

Nanostructures of ZnSe were grown on Si substrates in high vacuum (10^{-3} Pa) by thermal evaporation. The evaporation setup similar to the one used for the growth of MoO₃ nanowires was employed (Zhou et al. 2003; Yuvaraj et al. 2009). One gram of ZnSe granules (Cerac 99.99 %) was loaded onto the tantalum evaporation boat and covered with a perforated tantalum cover. Si substrates cleaned by acetone, de-ionized water and diluted hydrofluoric acid were placed over the perforated tantalum cover with an alumina spacer of 0.2 cm thick as shown schematically in Fig. 1. The temperature of the evaporation boat was calibrated prior to the experiment by an alumina tipped thermocouple. The vacuum chamber was initially evacuated to 1×10^{-3} Pa and the tantalum boat was heated to desired temperature (850, 900 and 950 °C) and held at this temperature for 4 min. After evaporation, Si substrates coated with fluffy yellow powder product were carefully removed and used as such for further morphological, structural and optical studies. Morphology and composition of ZnSe nano and microstructures were examined by SEM (ESEM Quanta) attached with energy dispersive X-ray analysis (EDAX) facility and its structural property was studied by XRD (Bruker D8, X-ray diffractometer). Microstructure

and chemical composition of the nanostructures were studied by TEM (Tecnai F30) and X-ray photoelectron spectroscopy (XPS, Multilab 2000). The PL spectra of the nano and microstructures grown at different source temperature was recorded at room temperature by ocean optics spectrophotometer using 325 nm He-Cd laser as excitation source.

Results and discussion

Morphological studies

ZnSe evaporated from the tantalum boat condenses on the Si substrate kept above the evaporation boat and grows into different nano and microstructures. ZnSe powder collected on the Si substrates at source temperature of 850 °C exhibited two distinct morphologies. The regions with different morphologies on the Si substrate are schematically marked as I and II in Fig. 1. Fig. 2a, b show the SEM image recorded in regions I and II on the Si substrates. Morphology of the grown product changes with respect to the distance from the orifice of the evaporation boat. Region I, which is directly above the orifice of the tantalum cover, contains randomly grown microcrystals (Fig. 2a). Region II surrounding region I (~ 0.3 cm from the center) contains nanostructures with different morphologies such as nanobelts and nanowires grown together as shown in Fig. 2b. The width of the nanobelts varied from 50 to 200 nm, while its length varied from 5 to 6 μ m. Further, the ends of the nano and microstructures were observed to be smooth and free from catalytic particle. The other growth temperatures such as 900 and 950 °C also resulted in the growth of ZnSe micro and nanostructures, similar to the one grown at 850 °C (Fig. 2), and hence they are not shown here.

Structural and compositional studies

XRD patterns of ZnSe nanostructures grown at different source temperatures (850, 900 and 950 °C) are shown in

Fig. 1 Schematic of the evaporation setup employed for growing ZnSe nano and microstructures

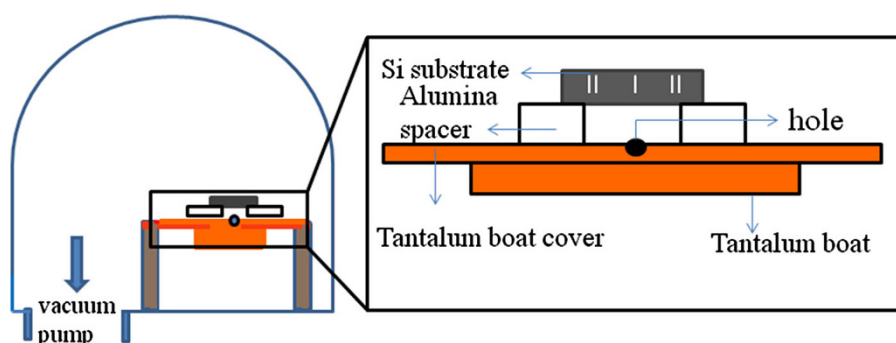


Fig. 2 **a** and **b** SEM images of ZnSe micro and nanostructures grown in regions I and II on Si substrate at source temperature 850 °C

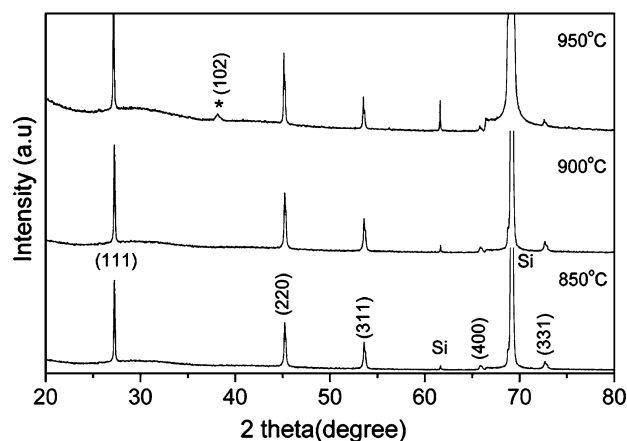
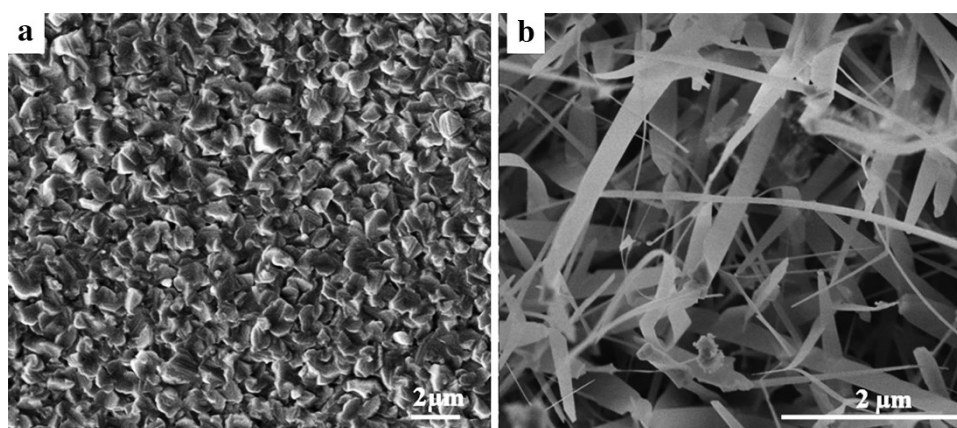


Fig. 3 Indexed XRD pattern of ZnSe nano and microstructures grown on Si substrates at different source temperatures

Fig. 3. XRD patterns were observed to be similar and these peaks were identified to that of the cubic phase of ZnSe, with lattice parameter $a = 0.5668$ nm (JCPDS No-371463). Further, impurity peaks or peaks corresponding to wurtzite phase of ZnSe were not observed in the samples grown at 850 and 900 °C. However, for the samples grown at 950 °C, a small peak corresponding to (102) wurtzite ZnSe phase was observed at $2\theta = 38.12^\circ$ (Fig. 3). Wurtzite phase of ZnSe is a metastable phase, which in bulk exists only at high temperature. The existence of stable wurtzite phase of ZnSe at room temperature in nanoscale has been reported (Hu et al. 2005). When ZnSe is evaporated at 950 °C, the high growth temperature favors formation of metastable wurtzite phase along with regular cubic zinc blende phase in grown nanostructures (Leung et al. 2006).

The chemical composition of the nanostructures was evaluated by EDAX during SEM analysis. Quantification of the EDAX spectra has shown the presence of Zn and Se in the atomic ratio ~ 1 . Further, compositional analysis of

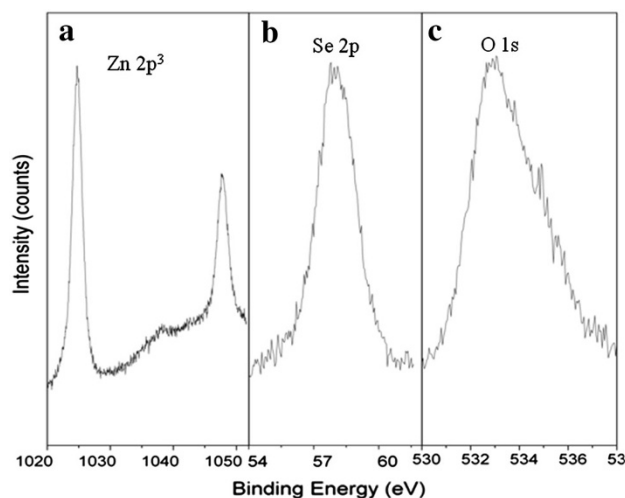


Fig. 4 XPS spectra of ZnSe nanostructures grown at 850 °C: **a** Zn 2p³ **b** Se 2p and **c** O 1s peaks

these nanostructures was carried out by XPS. The survey spectrum of the ZnSe nanostructures grown at 850 °C was recorded, then the binding energy obtained in the XPS spectra was corrected for the sample charging by taking C 1s at 284.6 eV as reference. The peaks corresponding to zinc, selenium and oxygen were identified from the survey spectrum (not shown here) and the extended spectra of these elements are shown in Fig. 4a–c. Figure 4a, b shows the peaks corresponding to that of Zn 2p³ and Se 2p at 1,024 and 57.3 eV, respectively. These peaks show that zinc and selenium present in the sample exist as compounds rather in the elemental form. The peak observed at 533 eV (Fig. 4c) corresponds to O–H bonds from the chemisorbed oxygen molecules on the surface of the nanostructure. Since the growth was carried out in high vacuum ($\sim 10^{-5}$ mbar), no strong peaks corresponding to the oxide layer at the surface of the nanostructures were observed.

Microstructural studies

Low magnification TEM image of belt-like nanostructure is shown in Fig. 5a. HRTEM image and its corresponding FFT pattern of the nanobelt are shown in Fig. 5b, c. HRTEM image shows good crystalline nature of the ZnSe nanobelt and also shows that the grown nanobelt is free from structural defects such as stacking faults and twins. The spacing between fringes in the image was measured using FFT pattern and it was found to be around ~ 0.328 nm. This d-spacing corresponds to the (111) of cubic ZnSe, as these lattice fringes are at an angle $\sim 35^\circ$ to the nanobelt growth axis, the probable growth direction of the nanobelt is identified to be along [110]. Similarly HRTEM analysis of other nanowires and belts also exhibited similar growth directions (HRTEM image not shown here).

Uniform distribution of nanoparticles on the surface and edges of nanobelts was observed during TEM analysis (Fig. 5b). The nature of these nanoparticles and composition of a nanowire was analyzed by electron energy loss spectroscopy (EELS) in scanning transmission electron microscope (STEM). Figure 6a shows the STEM image of a nanobelt exhibiting such morphology and the corresponding EELS elemental maps of zinc and selenium of the nanobelt are shown in Fig. 6b, c. Zinc mapping shows an even distribution of the element zinc all over the nanobelt, whereas selenium mapping shows the formation of selenium nanoparticles on the surface and in the edges of the nanobelt. These selenium particles are found to be so thin

that the HRTEM image of the nanobelt is unaffected by the presence of these particles (Fig. 5b). The formation of these selenium nanoparticles on the surface of the nanobelt is attributed to diffusion of selenium from the nanobelt during TEM studies. One-dimensional (1D) nanostructures have low melting point than their bulk counterparts. During TEM analysis, the incident high-energy electron beam loses a portion of kinetic energy via inelastic scattering, when transmitting through nanostructures which heats up the nanostructures under observation. Melting of nanowires such as Au, Zn, Si and Ge under electron beam irradiation has been reported (Shi et al. 2007). In our study, instead of melting, selenium atom diffuses out from the nanobelts to form selenium nanoparticles on the surface. The d-spacing in HRTEM images remains same and no change was observed as the result of selenium diffusion.

PL studies

PL spectra of ZnSe nanostructures grown at different source temperatures (850, 900 and 950 $^\circ\text{C}$) shown in Fig. 7 exhibited an intense broad and a weak narrow emission peaks. The weak emission peak at 464 nm (inset of Fig. 7) is attributed to the NBE emission and the broad intense emission peak from 550 to 850 nm to the DL emission. Although there are several reports available on the PL studies of ZnSe, yet the origin behind DL emission remains unclear (Basu et al. 2008; Philipose et al. 2008). The origin of DL emission has been related to the growth conditions, presence of non-stoichiometric point defects, incorporation

Fig. 5 a Low magnification TEM image of ZnSe nanobelt. (b and c) HRTEM image and its corresponding FFT pattern of the ZnSe nanobelt grown along [110]

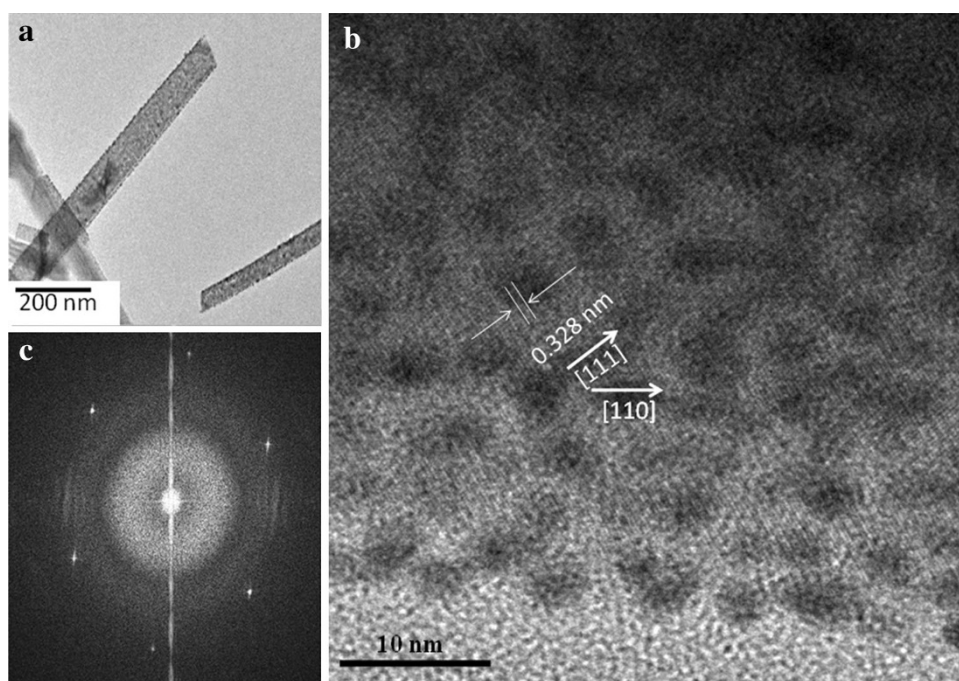


Fig. 6 **a** STEM image of ZnSe nanobelt. (**b** and **c**) Elemental maps of zinc and selenium recorded by EELS

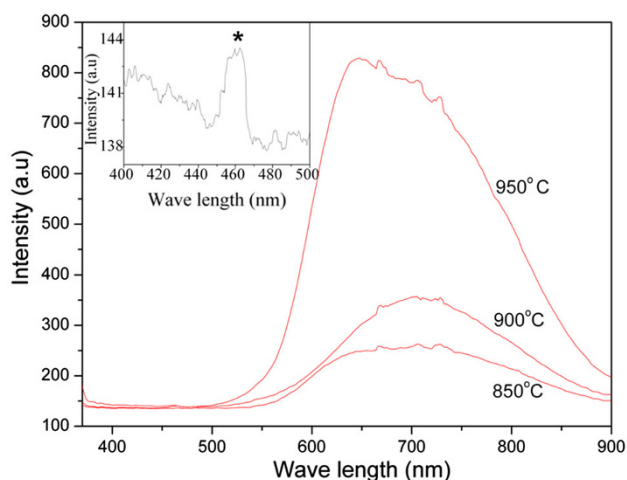
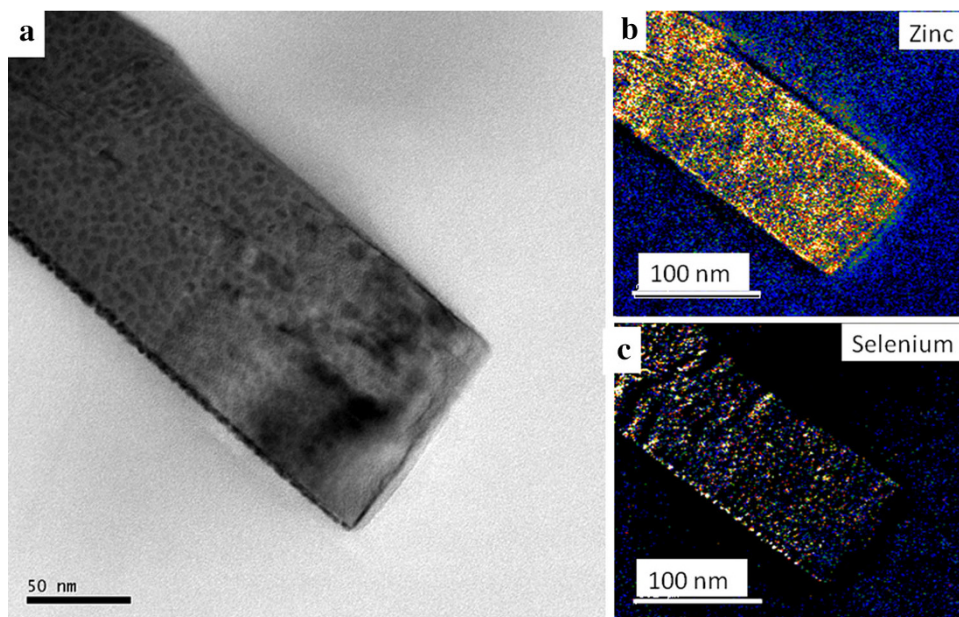


Fig. 7 Room temperature PL spectra of ZnSe nanostructures grown on Si substrate at different source temperatures (850, 900 and 950 °C). The magnified image of PL spectra corresponding to NBE emission is shown in the inset

of impurities and structural defects such as twin and stacking faults (Basu et al. 2008; Philipose et al. 2008). TEM studies on several such nanostructures grown at different temperatures have not shown the presence of structural defects such as twin and stacking faults. In our studies, nano and microstructures were grown at high vacuum; hence the effect due to incorporation of impurity has been lowered. Hence the strong DL emission may arise from non-stoichiometric point defects formed due to high growth temperature. Further it is observed that the intensity of DL emission peak was found to increase with the source temperature as a result of increase in the non-stoichiometric defects with respect to source temperature.

Growth mechanism

A wide range of nanostructures have been synthesized by vapor transport methods using horizontally aligned tubular furnace (Ye et al. 2004; Leung et al. 2006). The morphology of grown nanostructures was found to vary with source temperature, substrate temperature, partial pressure, carrier gas flow rate and nature of the starting material and catalyst (Jin et al. 2007; Zhai et al. 2007). Different growth mechanisms such as VLS, VS and VSS have been proposed to explain the growth of these nanostructures (Hu et al. 2005; Leung et al. 2006). However, in the horizontally aligned tubular furnace both the substrate temperature as well as the supersaturation ratio decreases from the center to the edge of the furnace, resulting in the growth of nanostructures with different morphologies at different regions of the furnace (Ye et al. 2005). As these two parameters (substrate temperature and supersaturation ratio) are interdependent on each other in a tubular furnace, their effect on morphology cannot be investigated independently in this technique (Ra et al. 2008; Ma et al. 2003). In our study, the effect of supersaturation and substrate temperature on morphology has been investigated separately. ZnSe powder with different morphologies was grown on Si substrates in a single experiment. The nano and microstructures grown at source temperature of 850 °C are shown in Fig. 2. Microstructural and compositional analyses ruled out the presence of catalytic particles on the tip of the grown ZnSe nanostructures and hence the growth of the nano and microstructures occurs by VS growth mechanism (Leung et al. 2006). The growth of nanostructures with different morphologies on the Si substrates at a constant substrate temperature is explained based on

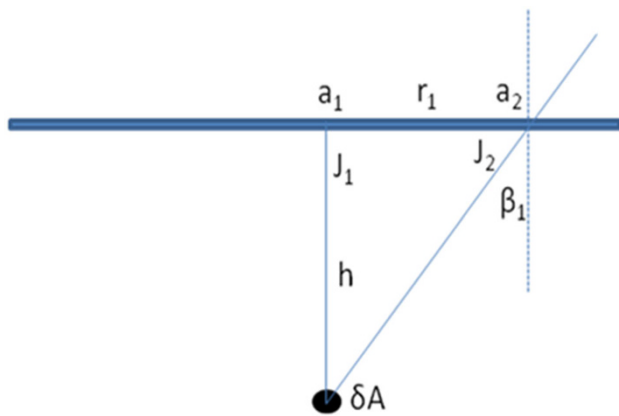


Fig. 8 Schematic of the substrates placed above evaporation boat (δA and h are $\sim 0.0314 \text{ cm}^2$ and $\sim 0.2 \text{ cm}$, respectively)

variation in the incident flux of ZnSe. Considering evaporation of ZnSe from the orifice (δA) of tantalum boat as a point source, incident flux at different position on the substrates was evaluated as shown in Fig. 8 (Mahan 2000). The beam intensity J_Ω ($\text{s}^{-1} \text{ steradians}^{-1}$) of the ZnSe source is given by Eq. (1).

$$J_\Omega = \frac{z\delta A \cos \theta}{\pi} \quad (1)$$

where θ is the emission angle, z (impingement rate) is given by $z = p/(2\pi mkT)^{(1/2)}$, where p is gas pressure, m is mass of the particle, k is Boltzmann's constant and T is source temperature. The incident flux (J_i) on the substrate placed at a distance of h from the center of the source is given by Eq. (2).

$$J_i = \frac{J_\Omega \cos \beta}{h^2} \quad (2)$$

where β is the deposition angle and h is the distance between the source (orifice) to the point of interest on the substrate. Incident flux (J_i) will be maximum at region I (a1) directly above the orifice, and the incident flux (J_i) decreases as a function of $\cos\beta$, from the center to the edges (a2). The supersaturation ratio (S) at a point on the substrate is calculated by Eq. (3).

$$S = \frac{J_i}{Z_{\text{eq}}(T_{\text{sub}}) - 1} \quad (3)$$

The supersaturation ratio (S) will be very high at region I as shown in Fig. 8 and decreases in similar manner to that of incident flux from region I to region II. Hence the formation of ZnSe with different morphologies in a single evaporation process is attributed only due to the variation in supersaturation ratio. The high supersaturation in region I resulted in the growth of microcrystal, whereas low supersaturation in region II gives rise to the growth of ZnSe nanowires and nanobelts by VS mechanism.

Evaporation of ZnSe at different temperatures such as 900 and 950 °C also resulted in the morphology similar to the one grown at 850 °C. It is observed from the present work that the morphology of the grown nano and microstructures of ZnSe was found to be highly dependent on the supersaturation ratio rather than on the source temperature in the investigated range 850–950 °C.

Conclusion

ZnSe nano and microstructures were grown in high vacuum by thermal evaporation process. SEM observation has shown that the morphology of grown structures was found to vary with supersaturation ratio at same substrate temperature, and high and low supersaturation ratios resulted in the formation of micro and nanostructures, respectively. Our investigation has shown that the source temperatures (850–950 °C) have less influence on morphology. TEM studies have shown that the grown nanobelts and wires are single crystalline in nature. Room temperature PL spectra of the ZnSe nanostructures have shown intense DL emission, and its ratio of DL to NBE emission strongly depends on source temperature. This modified high-vacuum thermal evaporation setup can be employed in future, to grow single crystalline nanostructures of other semiconducting and topological insulator materials.

Acknowledgments The authors sincerely thank the Institute of Nanoscience Initiative (INI), National Facility for Electron Microscopy, Indian Institute of Science, Bangalore, for providing facilities to carry out microstructural studies.

Open Access This article is distributed under the terms of the Creative Commons Attribution License which permits any use, distribution, and reproduction in any medium, provided the original author(s) and the source are credited.

References

- Basu J, Divakar R, Nowak J, Hofmann S, Colli A, Franciosi A, Carte CB (2008) Structure and growth mechanism of ZnSe nanowires. *J Appl Phys* 104(6):064302
- Cai Y, Chan SK, Sou IK, Chan YF, Su DS, Wang N (2006) The size-dependent growth direction of ZnSe nanowires. *Adv Mater* 18(1):109–114
- Hu J, Bando Y, Golberg D (2005) Sn-catalyzed thermal evaporation synthesis of tetrapod-branched ZnSe nanorod architectures. *Small* 1(1):95–99
- Jin L, Choy WCH, Leung YP, Yuk TI, Ong HC, Wang J (2007) Synthesis and analysis of abnormal wurtzite ZnSe nanowheels. *J Appl Phys* 102:044302
- Katayama K, Yao H, Nakanishi F, Doi H, Saegusa A, Okuda N, Yamada T, Matsubara H, Irikura M, Matsuoka T, Takebe T, Nishine S, Shirakawa T (1998) Lasing characteristics of low threshold ZnSe-based blue/green laser diodes grown on conductive ZnSe substrates. *Appl Phys Lett* 73(1):102–104

- Leung YP, Choy WCH, Markov I, Pang GKH, Ong HC, Yuk TI (2006) Synthesis of wurtzite ZnSe nanorings by thermal evaporation. *Appl Phys Lett* 88:183110
- Ma C, Moore D, Li J, Wang ZL (2003) Nanobelts, nanocombs, and nanowindmills of wurtzite ZnS. *Adv Mater* 15(3):228–231
- Mahan JE (2000) Physical vapor deposition of thin films. Wiley-Interscience, New York
- Mazher J, Shrivastav AK, Nandedkar RV, Pandey RK (2004) Strained ZnSe nanostructures investigated by X-ray diffraction, atomic force microscopy, transmission electron microscopy and optical absorption and luminescence spectroscopy. *Nanotechnology* 15(5):572–580
- Pal AK (1999) Size quantization effects in optical and electrical properties of II–VI semiconductor films in nanocrystalline form. *Bull Mater Sci* 22(3):341–351
- Philipose U, Saxena A, Ruda HE, Simpson PJ, Wang YQ, Kavanagh KL (2008) Defect studies of ZnSe nanowires. *Nanotechnology* 19:215715
- Ra HW, Choi KS, Hahn YB, Im YH (2008) The role of the vapor composition in the evolution from 1D to 2D ZnO nanostructures. *J Phys Chem C* 112:17926–17930
- Shan CX, Liu Z, Zhang XT, Wong CC, Hark SK (2006) Wurtzite ZnSe nanowires: growth, photoluminescence, and single-wire Raman properties. *Nanotechnology* 17(22):5561–5564
- Shen G, Chen D, Lee CJ (2006) Hierarchical saw-like ZnO nanobelt/ZnS nanowire heterostructures induced by polar surfaces. *J Phys Chem B* 110(32):15689–15693
- Shi L, Xu YM, Li Q, Wu ZY, Chen FR, Kai JJ (2007) Single crystalline ZnS nanotubes and their structural degradation under electron beam irradiation. *Appl Phys Lett* 90(21):211910
- Xiang B, Zhang HZ, Li GH, Yang FH, Su FH, Wang RM, Xu J, Lu GW, Sun XC, Zhao Q, Yu DP (2003) Green-light-emitting ZnSe nanowires fabricated via vapor phase growth. *Appl Phys Lett* 82(19):3330–3332
- Ye C, Fang X, Wang Y, Yan P, Zhao J, Zhang I (2004) Structural characterization of long ZnSe nanowires. *Appl Phys A Mater Sci Process* 79(1):113–115
- Ye C, Fang X, Hao Y, Teng X, Zhang L (2005) Zinc oxide nanostructures: morphology derivation and evolution. *J Phys Chem B* 109(42):19758–19765
- Yuvaraj D, Narasimha Rao K, Nanda KK (2009) Effect of oxygen partial pressure on the growth of zinc micro and nanostructures. *J Cryst Growth* 311(18):4329–4333
- Zhai T, Zhong H, Gu Z, Peng A, Fu H, Ma Y, Li Y, Yao J (2007) Manipulation of the morphology of ZnSe sub-micron structures using CdSe nanocrystals as the seeds. *J Phys Chem C* 111:2980–2986
- Zhou J, Deng SZ, Xu NS, Chen J, She JC, Wang ZL (2003) Large-area nanowire arrays of molybdenum and molybdenum oxides: synthesis and field emission properties. *Adv Mater* 15(21):1835–1840